# Friction and Wear Analysis of Shock Absorbers Using MR Fluid-Based Bio-Lubricant with Tergitol NP-10

*Stalin.*S.S[1], *Balamurugan.* P[1*],*Uthayakumar.* M[2], *Pethuraj.* M[3]

[1]Kalasalingam Academy of Research and Education, Department of Mechanical Engineering, Krishnankoil-626126.
[2]Amrita Vishwa Vidyapeetham, Department of Mechanical Engineering, Amritapuri 690525
[3]Saveetha School of Engineering, Department of Mechanical Engineering, Saveetha Institute of Medical and Technical Sciences, Chennai-602105.

**Abstract:** This study examined the friction and wear properties of organic oil-based magnetorheological (MR) fluids as bio-lubricants. Safflower Seed Oil (SSO) and Cashew Nut Shell Oil (CNSO) served as base fluids, each containing 0.3 µm iron particles and Tergitol NP-10 at 0.5–3 wt.%. Tribological performance, assessed via a four-ball machine, showed optimal results for SSO with 2.5 wt.% additives, yielding a wear scar diameter of 340 µm and a coefficient of friction of 0.0418. Real-world testing in 132 DG MR shock absorbers under varying electromagnetic fields, motion amplitudes, and frequencies revealed damping force errors of 9% (SSO, 2.5 wt.%) and 10% (CNSO, 2 wt.%), supported by finite element analysis. Molecular-level evaluation using Wavefunction Spartan 18 provided insights into tribological mechanisms. Wear progression was noted, with cylindrical wall diameters increasing by 3.36 µm after 96 hours of operation. Overall, 2.5 wt.% SSO demonstrated superior wear resistance and damping performance over other formulations, highlighting the potential of organic MR fluids as environmentally friendly alternatives for mechanical systems such as shock absorbers, combining improved performance with sustainability benefits.

## 1 Introduction

A carrier fluid which typically comprises an oil solution acts as the foundation for Magnetorheological fluid (MR fluid). The fluid changes into a viscoelastic solid following exposure to magnetic fields because its viscosity rises significantly [1]. The active state yield stress of the liquid depends precisely on magnetic field strength variation [2]. When a magnetic field activates MR fluid the viscosity increases since its micrometer-sized particles exceed the carrier fluid density threshold for sustaining Brownian motion suspension [3]. The first portion of this text provides fundamental information about MR fluid properties and shows different application-oriented MR fluid devices. The section introduces several future applications of MR fluids which emerged recently [4]. The three operational modes of MR

[1]Corresponding author: pbala.klumech@gmail.com

fluid exist as flow mode and shear mode with squeeze flow mode being the third possibility [5]. The fluid moves in three operational modes under conditions where one plate is stationary and the other two plates operate at different levels of relative motion or perpendicular motion to their planes [6]. The magnetic field remains perpendicular to every plate plane which enables fluid retention in the parallel direction. The ERF needs thousands of volts coupled with few mA of current whereas the MRF system functions with a power range of 2 to 24 volts and several amps. The electro-rheological (ER) effect requires application of electrostatic fields but magneto-rheological (MR) effect works through magnetic fields. MRF technology provides a greater degree of control through its products which display a control effect that exceeds ERF components by twenty to fifty times [7].

A base fluid serving as the carrier oil maintains a vital function for modifying MR fluid properties because it constitutes the predominant fluid portion (50%-80% by volume) [8]. Machine parts fail because of wear and friction since MR fluid lacks enough lubrication from its iron particles components [9]. Silicon oil-based MR fluid is a subject that multiple research teams have continuously examined. The research compares the bio-lubricants to current industrial 132DG MR Fluid standards and tests their performance both during experimental measurements and actual application conditions with the addition of friction and wear tests [10]. The four-ball tribological evaluations of CNSO oil and SSO oil need to continue under ASTM D4172 B with and without additive presence. Both vegetable oil formulations are evaluated as lubricating oil in shock absorbers to measure bore diameter changes by using a coordinate measuring machine against 132DG MR Fluid as reference. A study examined how the integrated magnetic shielding layer affects magnetic fields through modeling of shock-absorbers which implemented single cylinder shielding together with sandwich cylinder shielding structures [11]. A model of the shock-absorber's magnetic field operated through finite element software simulation. The comparison between experimental measurement and computer simulation data indicated minimum errors at 8.2% and maximum errors at 15% [12]. Multiple damping channels interconnected with each other extended the liquid flow damping length when the shock-absorber piston moved along them. The design realization results indicate that the shock-absorber structure optimizes the magnetic flux usage for increasing damping output. The design phase analysis of magnetic fields in this research involved the evaluation of one single physical field. The fluid MR properties lead the MR shock-absorber to operate as a complex system between electromagnetic fields and hydraulic systems with solid mechanical elements. The system performs under the effects of multiple physical domains due to multi-physics phenomena [13,14]. Wave-function Inc (US) provides the software Spartan 18 for this application. Software has two main capabilities which enable users to both discover molecular arrangement and compute chemical characteristics. The tool enables scientists to describe different phenomena by studying molecular-level changes. The program enables users to evaluate Molecular orbital energy and Net electrostatic charge values that lead to specific oil behaviour explanations [15].

## 2 Experimental Details

### 2.1 Materials:

Amid organic oil-based lubricants, the safflower seed oil and cashew nut shell oil are used as a carrier fluid. Organic oil was procured from Saptham food & beverage Pvt Ltd, Bangalore. Wear rate is a function of iron particles size depended, if iron particle size increase wear rate also increases, hence to obtain optimum size iron powder from Nice chemicals Pvt Ltd, Pune. Tergitol NP -10 purchased from Sigma-Aldrich chemicals private Ltd, Bangalore, it having 99.5% of purity. Tergitol NP-10 is used as additives with different Wt.% of the surfactant to scattering particles in the carrier fluid. 132DG MR fluid was procured from the Lord Corporation, United States of America.

### 2.2 Synthesis of MR Fluids:

In the current investigation, MR fluid has three rudiments segment: base fluid, magnetic particles and additives. MR fluid make ready starts with base fluid that is Organic oil, Tergitol NP-10 and the iron powder coated with lithium Grease. Two variety of organic oil were engaged with this study, that oil names are safflower seed oil (SSO) and Cashew nut shell oil (CNSO) the physical properties of the oil are listed in Table 1.The Dynamic viscosity was determined through a Rheometer - Anton Paar and Consistency of oil measure by conventional method weight by volume ratio, whereas fire and flash point value measured from Apel Apparatus in this all experiment conducted at a temperature 300°C. Often the molecules size of iron molecules dispersed in the MR fluid various starting with 1µm to 10µm.

**Table 1.** Physical Properties of Carrier oil.

| | **Viscosity (Pa.s)** | **Density (g/cm$^3$)** | **Flash Point °C** | **Fire point °C** | **Réfractive Index** |
|---|---|---|---|---|---|
| Safflower seed oil (SSO) | 0.045 | 0.94 | 315 | 375 | 1.469 |
| Cashew Nut shell oil (CNSO) | 0.353 | 1.009 | 172 | 205 | 1.515 |
| Silicon oil | 0.34 | 0.95 | 300 | 350 | 1.404 |

The iron particles size increase with increase in sedimentation where as our experiment used average 0.35µm size with spherical shape and the sample were taken 30Wt.% Additives are classified as stabilizers and surfactants; here stabilizers are act as lithium Grease 0.793gm/cm$^3$ and Flash point 165°C.Lithium Grease act as coating agent it's helped to keep the iron particles suspended in a carrier fluid, whereas Tergitol NP-10 as the surfactants to disperse iron particles throughout the carrier fluid whereas in different concentration of Wt.% like 0.5, 1, 1.5, 2, 2.5 and 3 Wt.%.

1) Iron 99.56% purity particles and Tergitol NP-10 was added part by part in 10 steps and then stirrer at 600rpm with 3hr.
2) Then, lithium grease was added and stirrer for another 3hr at 600rpm.
3) The carrier fluid SSO and CNSO oil was added to the mixture of above parts stirrer another 3hr at 600rpm.

Various samples of MR fluid were synthesized with different concentration of SSO, CNSO, Lithium Grease, and Tergitol NP-10. The percentage of Lithium Grease in the all samples is 10 Wt.%. By Using this synthesis method, the particle was coated with Lithium Grease which is better as the dispersion of the magnetic iron particles in the working fluid, the coated particles which also helpful for the particle suspension. Under different composition of organic oil-based MR fluid were studied in sedimentation ratio, also the Yield stress and fluid flow character were measured by magneto- Rheometer, safflower seed oil with 2.5% of TL in this composition had improve sedimentation as well as stability compare with experimental test result.

### 2.3 Friction and Wear Test:

Evaluate the different tribological properties of bio-lubricant based Fluid such as Wear Preventive Test, COF, and Extreme pressure by contacting tests on an ASTM D2266 standard. In Ducom Instrumentations Private Ltd, Banglore, India, this contains four ball test rig as shown in Fig 1. The balls diameter is 12.7mm it's made up of Chromium steel, weight 8.3563gms and 64HN hardness. The test is done using unique sample configuration of three lower balls and one top ball which makes a repeatable contact in turn and very stable, which allows the test results to be repeatable. The four-ball tester with magnetic field passing through insulated coil wire with 0.9mm diameter, voltage (20-40V) and current 2A, respectively. A coil of wire acts as a magnet when an electric current flow it. In the magnetic moment test (M-B curve) magnetic density varied from 0 to more than 1.5 Tesla. The optimum magnetic flux density 1.36T get from B-M curve, in which flux density is constant and change the other concentration to determine the wear and friction. During testing, the steel balls are immersed in lubricant and a routing steel ball is pressed against three steel balls firmly held together. During anti wear test to be maintain standard method like load, time period, speed of rotational and temperature are set in accordance with quality test method. Preventive wear test called as an Anti-wear test, where calculated wear value an average three ball scar dimension is recorded. Prevent wear character vary based on dimension of the ball scar. Preventive wear character indicates badly off, when ball scar dimension is huge while low ball scar dimension indicates good preventive wear character. The rheological character of base oil SSO and CNSO with additives in different concentration of Wt% like 0.5, 1, 1.5, 2, 2.5 and 3 Wt%, whereas test result in wear scar diameter as shown in Fig 2 and 3. The chromium steel ball make a contact in point displayed in figure.1. The angle of touch b/w the ball was 35.2650. For wear scar test, the upward force was 30kgf (i.e., 295 N), where P is upward force, L is the net force on lower balls, L=3F, F is the actual force per each lower balls (F= 0.40823P), the calculated value of each lower ball is 12kgf from Eq. (1).

$$P = L\cos\theta \quad (1)$$

The maximum exposure pressure (i.e. the Hertzian stress) has been calculated and the mean contact pressure is two thirds of the maximum exposure pressure.

$$\frac{1}{r} = \frac{1}{r1} + \frac{1}{r2} \quad (2)$$

$$\frac{1}{Y} = \frac{1-\gamma 1^2}{Y1} + \frac{1-\gamma 2^2}{Y2} \quad (3)$$

$$P_1 = \frac{1}{\pi}\left[\frac{6FY^2}{r^2}\right]^{1/3} \quad (4)$$

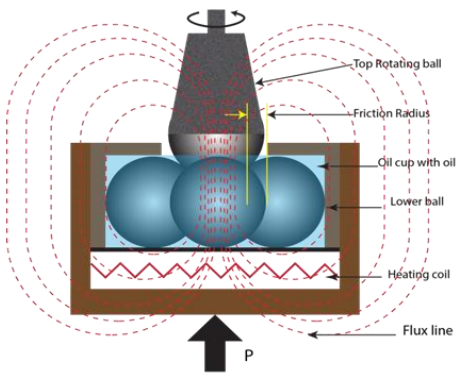


**Fig. 1.** Schematic diagram of Test rig.

Where r, r1, r2 are the effective radius and the radius of the upper and lower sphere respectively. Y,Y1,Y2 and γ,γ1,γ2 are the young modulus (200GPa) and passion ratio (0.3), above the values are substituted equation(2), (3) and (4). The calculated value of maximum contact pressure 3078Mpa from Equation (4) respectively.

**Fig. 2.** Wear scar diameter of (a) Without Field CNSO + 2.5wt% TL (b) CNSO + 1wt% TL (c) CNSO + 1.5wt% TL(d) CNSO + 2wt% TL (e) CNSO + 2.5wt% TL (f) CNSO + 3wt% TL

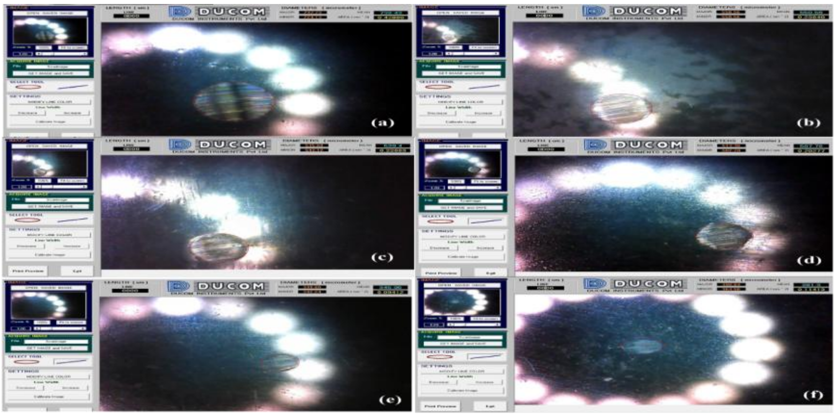

**Fig. 3.** Wear scar diameter of (a) Without field SSO+2.5wt% (b) SSO + 1wt% TL (c) SSO + 1.5wt% TL(d) SSO + 2wt% TL (e) SSO + 2.5wt% TL (f) SSO + 3wt% TL

The scar viewer software is used to capture image were as shown in Fig.2 and Fig.3, which measure Wear Scar Diameter (WSD) and displays the Coefficient of friction (COF) in Fig. 6. When the magnetic flux density was 1.36T, the average wear scar diameter degreases from 756 µm (max) to 392µm (min) it's the combination of CNSO oil + additives with magnetic flux density. The maximum wear scar diameter scored to CNSO+0.5 W.% TL, minimum diameter CNSO + 2 Wt.% TL and 388µm obtained CNSO + 2 Wt.% TL without magnetic flux density. Similarly, where, Safflower oil-based MR fluid wear diameter value observed the value reduced from 726µm (max) to 349µm (min). The maximum wear scar diameter scored to SSO + 0.5 Wt.% TL, minimum diameter SSO+ 2.5wt %TL and 332µm obtained SSO + 2.5 Wt.% TL without magnetic flux density. In the base oil, the iron particles are dispersed freely when the field is off, and they can take part in the abrasion and wear of contact point which cause serious wear without magnetic field. These iron particles are adsorbing in a line or aggregate when the field is on. Compared to the absence of magnetic induction, the viscosity of MRF is higher.

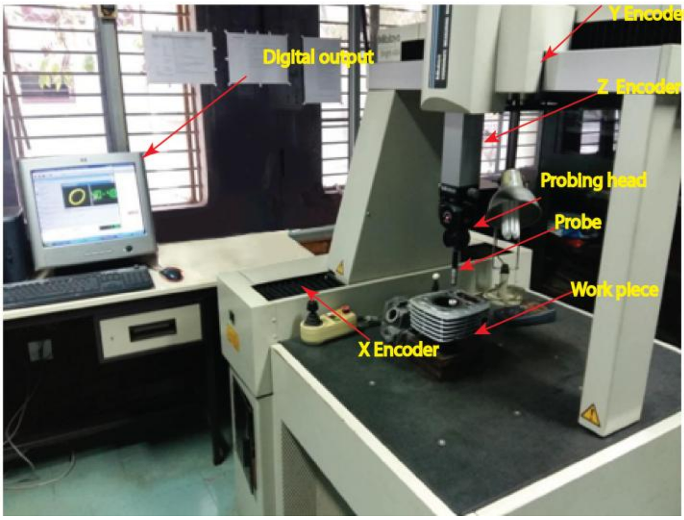


**Fig. 4.** Coordinate Measuring Machine

### 2.4 Tribological Test on Cylindrical Wall:

A Coordinate measuring machine (Bright-A504, X 505, Y 405, Z 405, Mitutoyo, Japan) operates as a device to measure physical object geometry through probe sensing of surface points. After the shock-absorber construction the device moves to the CMM table where inspectors perform their measurements for software-assisted process adjustments when workpiece variations occur. The probing instrument located on the third movable axis (Z axis) of this machine performs the measurements. This measurement device reaches accuracy levels of 0.5 micrometres in its measurements. The automated laboratory device at the NITC lab in India operates by receiving programmed codes to run independent measurements. The probe created 48 separate measurements at each depth position of 5 mm during the conducted test. The diameter results from combining 48 points of measurement that cover the entire stroke length by increments of 5 mm each. The CMM probe along with its stylus enters the hole to reach and touch the shock-absorber cylinder wall following which the machine proceeds to a new position for establishment of coordinates for that specific area of contact. The computer receives specific XYZ locations from the software that enables it to determine the cylinder wall diameter changes before and after 96 hours.

## 3 Results and Discussion

### 3.1 Anti-Wear Inspection:

The wear scar diameter value difference are plotted in Fig.5 for variable proposition of additives, where Tergitol NP-10 and base oil (SSO and CNSO). The concentration of 0.5, 1, 1.5, 2., 2.5 and 3Wt% of additives. From Fig. 5 it can be observed that there is continuous decrease of WSD with the increase of the amount of Tergitol from 0% to 3 % and then it increases. From this we get that the minimum wear scar diameter is found out when 2% TL by weight is added to CNSO oil and onward increase of TL would lead to increase in wear as excess TL, which cannot bond to the oil, would serve as abrasive and expedite the wear while hampers the tribo film formation. Fig.5 demonstrates the fact that WSD continuously decreases as the concentration of TL increases from zero percent to three percent, after which it starts increasing. This gives us that it is at the concentration of 2.5% of TL by weight in SSO oil where we obtain the minimum wear scar diameter and as the concentration of TergitolNP-10 increases the wear will further increase, since the excess TL in that case would act as abrasive and speed the wear process and is detrimental to the formation of tribofilm. Comparison among the wear properties of all the oils at various proportions can be easily made [20]. Based on the field parameter of WSD, the best result as per four ball tests is for SSO oil with 2.5 wt% TL. The variation of TL concentration of CNSO oil with respect to variation of concentration of TL has a more linear and stable variation. Both of them increase WSD after an optimum concentration point.

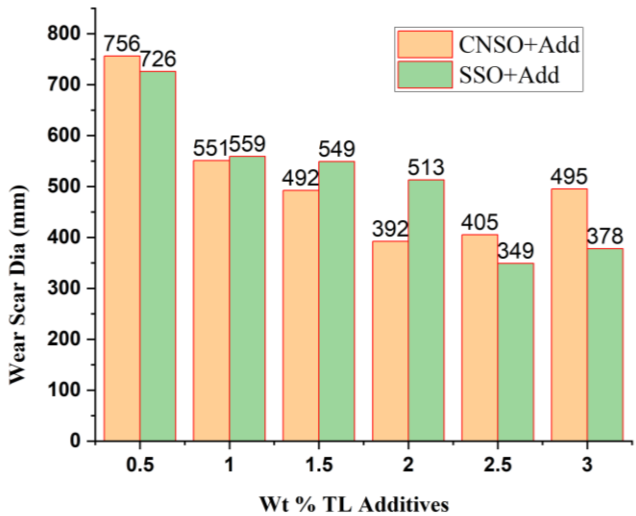


**Fig. 5.** 5 WSD vs Wt. % TL comparison graph

### 3.2 Co-efficient of Friction

Friction acts as the oppositional force which resists motion between solid objects plus between sliding or rolling elements made from either solids or liquids. The mathematical expression of the force of friction between two bodies and the force acting on them appears as a dimensionless scalar quantity termed the coefficient of friction (COF) which uses the Greek symbol μ. The coefficient experiences values that exceed those of its corresponding kinetic value. The relative motion friction coefficient equals the kinetic coefficient of friction when motion occurs. The stable and average friction value rose from 0.0434 to 0.611 based on the Tergitol concentration weight percentage under a magnetic field of 1.36T. Subjecting the magnetic flux density to an increase produces a friction value that reaches five times higher than the base quantity of no magnetic field. The higher magnetic field intensity was induced into high viscosity, similarly high friction but lesser wear. The maximum coefficient of friction value 0.588 it's the combination of CNSO+0.5 wt.% TL, minimum value 0.391 of COF is CNSO+ 2wt %TL and 0.0434 obtained CNSO+2wt%TL without magnetic flux density. Similarly, where, Safflower oil-based MR fluid COF value observed the value reduced from 0.611 (max) to 0.332 (min). The maximum coefficient friction scored to SSO+0.5 wt.% TL, minimum COF occurs SSO+ 2.5wt %TL and 0.0438 obtained SSO+2.5wt%TL without magnetic flux density from the Fig.6. It concluded that anti-wear ability and friction reduction of CNSO+2Wt%TL is better than SSO+2.5Wt%TL.

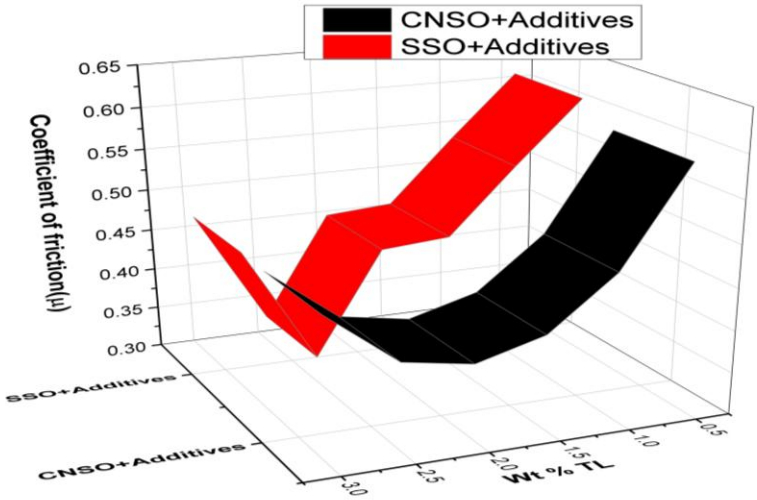


**Fig. 6.** Coefficient of friction as a function of the weight fraction TL in the different oils

### 3.3 Wear Analysis on Cylindrical Wall Surface

The cylinder is disassembled from the assembled shock-absorber and measure the geometrical dimension by using CMM machine. The cylinder inner diameter (D1=60mm), rod size (d=15mm) and Stroke length (l1=70mm). First, we consider 132DG MR fluid are filed in the shock-absorber. The shock-absorber was tested 96hr at frequency (f= 1.5Hz) and at an approximate load of 400N. The test results were as shown in Fig.7 as well as table.2. We see that the increase in diameter, average is 3.64 µm, and then another two concentrations of oil were filled in shock-absorber one by one, similar procedure is followed to run the shock-absorber.

**Table 2.** Cylinder wall diameters before and after 96hr running by using CMM

| S.No | Stroke Length Distance from TDC | Cylinder dia before running(mm) | Cylinder dia After running 96 hr | Increase in diameter | Cylinder dia before running(mm) | Cylinder dia After running 96 hr | Increase in diameter | Cylinder dia before running(mm) | Cylinder dia After running 96 hr | Increase in diameter |
|---|---|---|---|---|---|---|---|---|---|---|
| 132 DG MRF OIL | | | | | CNSO Oil + 2Wt% TL | | | SSO Oil + 2.5Wt% TL | | |
| 1 | 1 | 60.003 | 60.007 | 3.806 | 60.002 | 60.007 | 5.022 | 60.009 | 60.013 | 3.88 |
| 2 | 6 | 60.002 | 60.005 | 3.701 | 60.005 | 60.009 | 4.838 | 60.010 | 60.013 | 3.78 |
| 3 | 11 | 60.002 | 60.006 | 3.609 | 60.004 | 60.009 | 4.718 | 60.010 | 60.013 | 3.72 |
| 4 | 16 | 60.001 | 60.005 | 3.584 | 60.004 | 60.009 | 4.658 | 60.002 | 60.006 | 3.69 |

| | | | | | | | | | | |
|---|---|---|---|---|---|---|---|---|---|---|
| 5 | 21 | 60.003 | 60.007 | 3.514 | 60.006 | 60.010 | 4.566 | 60.002 | 60.005 | 3.61 |
| 6 | 26 | 60.004 | 60.007 | 3.423 | 60.004 | 60.009 | 4.453 | 60.002 | 60.006 | 3.56 |
| 7 | 31 | 60.002 | 60.005 | 3.320 | 60.002 | 60.006 | 4.367 | 60.001 | 60.005 | 3.41 |
| 8 | 36 | 60.002 | 60.005 | 3.270 | 60.004 | 60.009 | 4.387 | 60.002 | 60.005 | 3.38 |
| 9 | 41 | 60.003 | 60.006 | 3.335 | 60.001 | 60.006 | 4.683 | 60.003 | 60.007 | 3.44 |
| 10 | 46 | 60.002 | 60.006 | 3.522 | 60.001 | 60.006 | 4.772 | 60.004 | 60.008 | 3.51 |
| 11 | 51 | 60.004 | 60.007 | 3.723 | 60.002 | 60.007 | 4.897 | 60.004 | 60.008 | 3.69 |
| 12 | 56 | 60.004 | 60.008 | 3.819 | 60.001 | 60.006 | 5.053 | 60.003 | 60.007 | 3.79 |
| 13 | 61 | 60.003 | 60.007 | 3.839 | 60.002 | 60.008 | 5.119 | 60.004 | 60.008 | 3.85 |
| 14 | 66 | 60.001 | 60.005 | 3.894 | 60.004 | 60.010 | 5.353 | 60.004 | 60.008 | 3.95 |
| 15 | 71 | 60.001 | 60.006 | 4.302 | 60.006 | 60.010 | 5.421 | 60.003 | 60.007 | 4.06 |
| Average increase in diameter | | | 3.64 µm | | 4.82 µm | | | 3.36 µm | | |

There is a significant increase in the cylinder bore diameter, average 0.486mm by using (CNSO+2Wt%TL) with length of the stroke. From the table. 2 there is significant increase in the bore diameter taking place. The diameter is seen to be more worn out near the Top and bottom of the stroke length region of the cylinder. The next experimentation is to use the SSO+2.5 Wt.% TL. It was observed that the increased wear was near the top and bottom of stroke length of the cylinder, the compare with middle portion of the cylinder. It's happening there based on the viscosity of the fluid. When magnetic induction increases also increase in viscosity of MR fluid. Top and bottom region of cylinder wall their magnetic Intensity is slightly poor compare with middle region. The findings are equivalent to industrial oil standards, which paves up the opportunity for additional advancements that could eventually result in the commercial manufacture of a lubricant version based on these vegetable oils and additives.

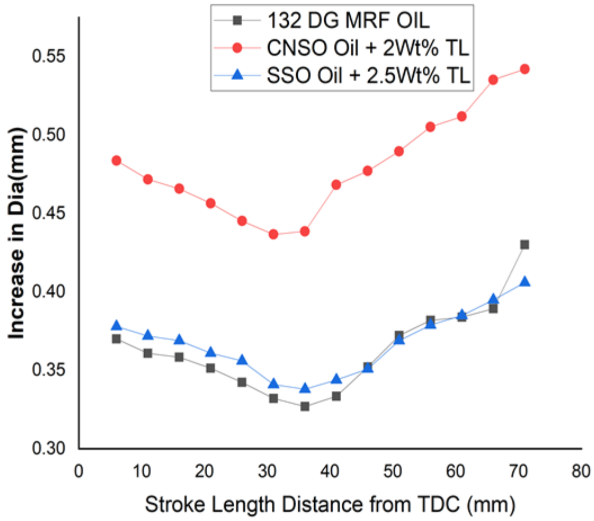


**Fig. 7.** Increase in cylinder wall diameter

### 3.4 Performance Analysis of Proposed MR Shock-absorber

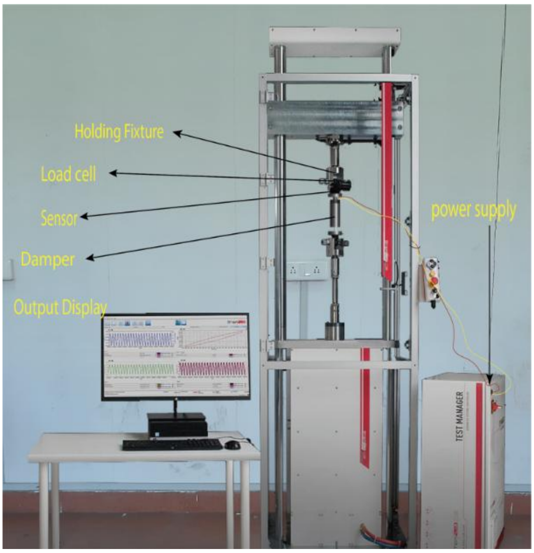


**Fig. 8.** Experimental Test Rig

Fig: 8, shoes that the experimental test system was mainly used for the shock-absorber, the proposed MR Shock-absorber based on vibration excitation. Bluehill universal materials testing software from Instron, purely computer-based testing system. Proposed MR shock-absorber was tested to analyse damping force and response for a set of inputs currents. The proposed shock-absorber were connected in UTM the upper end of shock-absorber was connected with hydraulic actuator they can move upward and downward motion, bottom end was connected with fixed flat form. The vibration excitation platform has an actuator, it's get Power supply given to the shock-absorber with various vibration excitations current. The findings are equivalent to industrial oil standards, which paves up the opportunity for additional advancements that could eventually result in the commercial manufacture of a lubricant version based on these vegetable oils and additives.

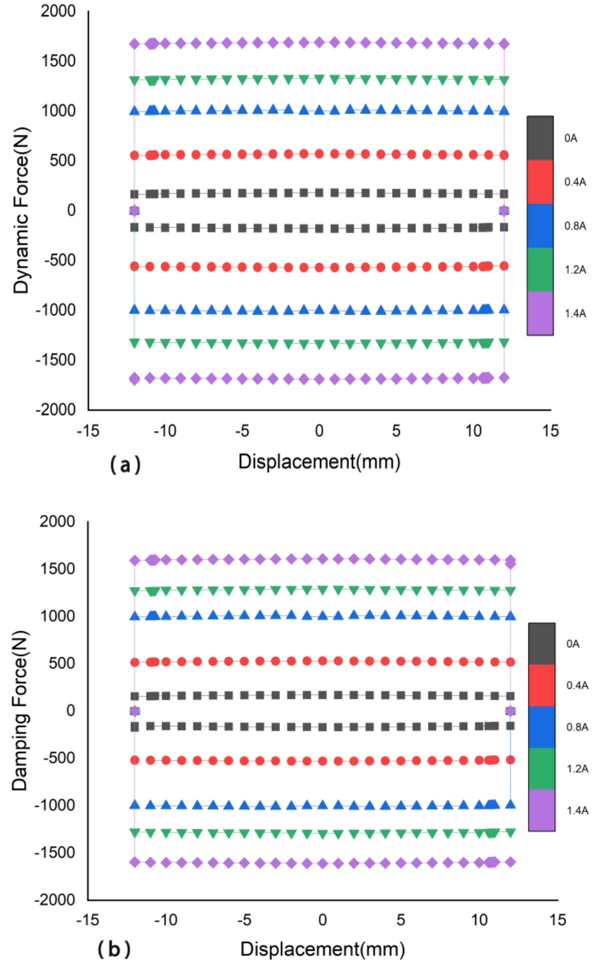


**Fig. 9.** Simulation Analyses in Various Parameter (a) SSO+2.5wt%TL (b) CNSO+2Wt%TL

The Summation of the responsive forces of the MR fluid on the piston is the output damping force of the shock-absorber. Immediately upon the shock-absorber is subjected to the vibration excitation with an amplitude of 12mm, frequency of 1 Hz and Voltage 2 V, here voltage and frequency were constant current varied from 0A to 1.4 A

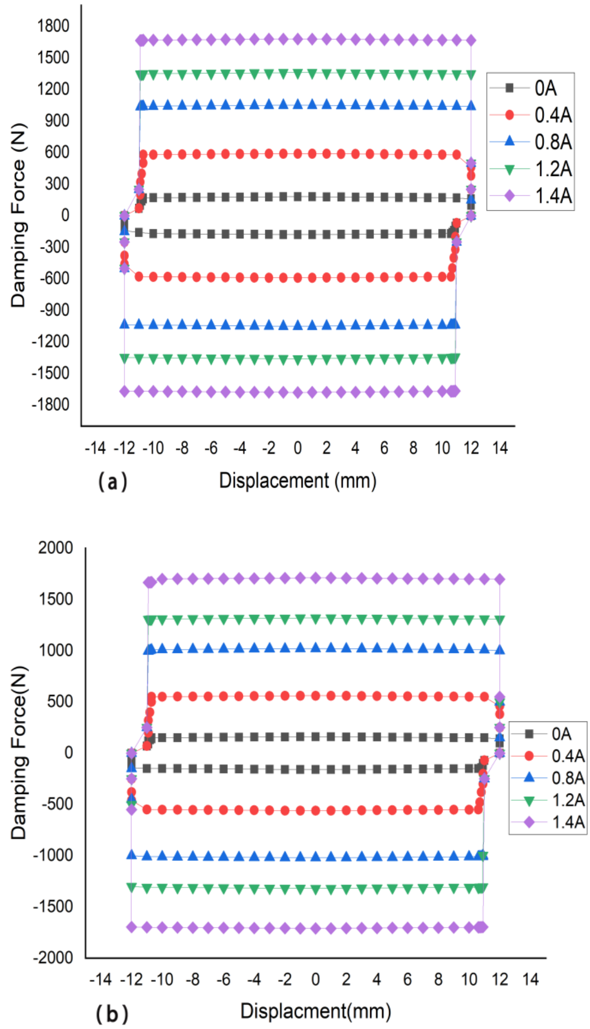


**Fig. 10.** Experimental analyses in Various Parameters (a) SSO+2.5 Wt.% TL (b) CNSO + 2 Wt.% TL

For simulation analysis of proposed MR shock-absorber is done by the multi-physics simulation finite element analysis software which gives the preference to dynamic performance of shock-absorber. The performance of MR shock-absorber is similar to its electromagnetic field which is energized with its field flow distribution and flow field of the shock-absorber. Fig 9 shows the output of resisting energy with displacement; the curve varies when different current is applied on the shock-absorber. By comparing the resisting energy and displacement graph for different current values, it shows the graph in which the resisting energy of proposed shock- absorber will be increases when the current gets increased. Magnetic saturation of the MR shock-absorber, just after the current reaches 1.4 A the resisting energy gets lower increment with increase in current.

**Table 3.** Design Specification

| Damper Specification | Dimension | Damper Specification | Dimension |
|---|---|---|---|
| Cylinder length/cm | 15.0 | Diameter of the piston pin /cm | 1.5 |
| Stroke /cm | 7.0 | Thickness of the damping gap /cm | 0.122 |
| Number of bobbins | 2 | Depth of the bobbin /mm | 35 |
| Turns of coil / nos | 1160 | Copper wire / Swg | 26 |

In this study, consider two types of oil 1.SSO+2.5wt%T and CNSO+2Wt%TL, both oils have different fluid properties, the output and resisting force ratio of a MR shock-absorber are the main performance indicators of its design. The former is the ratio of the force generated by the damping to the viscosity-induced force, while the latter is the resisting force ratio. For SSO+2.5wt%TL, When the current is 0 A, the viscous resisting energy in a MR shock-absorber is only 182.1 N, and its output is up to 1690 N when the current is 1.4A and the resisting force ratio is up to 9.28. For, CNSO+2Wt%TL When the current is 0 A, the resisting energy in a MR shock-absorber is only 178.2 N, and its output is up to 1610 N when the current is 1.4 A, and the resisting force ratio is up to 9.04. In the counterfeit analysis, the proposed shock-absorber can produce a resisting energy that is appropriate for an automobile shock absorber. According to the design specification in Table 3 and dynamic performance analysis of proposed shock-absorber in Fig:8. To conduct exploratory the role of different current on the resisting energy, the amplitude of the motion 12mm and frequency 1 Hz and input current varying from 0 A to 1.4 A. The experimentally conducted measured the value relation between resisting energy and displacement under different current, as shown in Figure 10. In the graph, we can saw resisting energy in proposed shock-absorber varies a little bit with displacement, they had twist appearing in the curve were mainly under poor vibration excitation during conducting exploratory. When magnetic flux density will be increase at the same time resisting energy also increase, more over once reached magnetic saturation of the MR shock-absorber, the resisting energy increase becomes lower with increase in current just after the current reaches 1.4 A. Additionally, the experiment and counterfeit analysis graph have same magnification. For SSO+2.5wt%TL, When the current is 0 A, the resisting energy in a MR shock-absorber is only 170 N, and its output is up to 1780 N when the current is 1.4 A, and the resisting force ratio is up to 10.47. For, CNSO+2Wt%TL When the current is 0 A, the resisting energy in a MR shock-absorber is only 160 N, and its output is up to 1710 N when the current is 1.4 A, and the resisting force ratio is up to 10.05. The resisting force ratio and vibration excitation resisting energy measured under various current condition same changing in the counterfeit analysis and experimentally, experimental value slightly higher than the counterfeit analysis value. It's occurring based on internal frictions of the shock-absorber were increased assembly errors of shock-absorber. For SSO+2.5wt%TL, the resisting energy error is 9% and the resisting force ratio error is 10.2% For CNSO+2Wt%TL, the damping force error is 10% only and resisting force ratio error is 10%. Compare the value of resisting force ratio and resisting energy for SSO and CNSO, SSO results were higher than CNSO because SSO had a high viscous force.

### 3.5 Wave Function Spartan Analysis:

Wave function Spartan 18 which helps us to explain the behaviour of these oils from the molecular level of analysis. Spartan software can be measuring the molecular structure shape, computational quantum analysis, structure optimization, atomic properties, electrostatic potential map and density functional theory etc. Carboxylic acids, as we have seen with aldehydes and ketones, have a longer carbon chain, but instead of a hydrogen as with aldehydes or a different carbon chain as with ketones, we have a OH group that is more acidic than alcohols because it loses its hydrogen once. If you put this in a solution of water, you have some $H_2O$.

**Table 4.** Net electrostatic charge of constituent acids

| Constituent Acid | Percentage of constituent acid | | Net Electrostatic charge on polar head group (Qr) |
|---|---|---|---|
| | SSO OIL | CNSO OIL | |
| Oleic Acid | 51.6 | 44.5 | -0.658 |
| Stearic Acid | 16.6 | 18.3 | -0.635 |
| Palmitic Acid | 11.65 | 18.1 | -0.655 |
| Linoleic Acid | 7.5 | 18.1 | -0.64 |
| Docosasnoic Acid | 4.4 | - | -0.638 |

As soon as the electron is given back to the oxygen molecules or to the water molecules, it gives one of its electrodes to a hydrogen proton and becomes positive. The carboxylic acid iron, which has taken an extra electron from the oxygen, has obtained two lone pairs, with one valence electron being negatively charged and is called iron hydronium. This one water molecule is now a hydronium molecule that has bonded with the hydrogen proton and now has a positive charge. It is more stable. Here net Electrostatic charge quantum value determines by using semi-empirical method. Here have less wear properties because the Fatty acids linoleic acid and stearic acid have lower net electrostatic charge on polar head group, here oxygen molecules indicate in red colour.

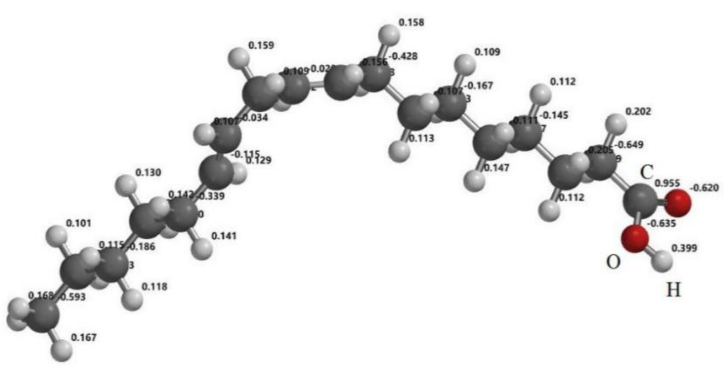


**Fig. 10.** Stearic acid Net electrostatic charges on atom.

## 4 Conclusion

- The tribological performance of SSO (Sesame Seed Oil) and CNSO (Cashew Nutshell Oil) was evaluated against the industrial standard 132DG MR fluid, with varying concentrations of Tergitol-NP10 as an additive.
- Among the tested combinations, SSO + 2.5 wt.% Tergitol-NP10 exhibited the lowest wear scar diameter and minimal cylinder wall wear, indicating superior anti-wear performance.

- The enhancement in tribological properties is attributed to Tergitol-NP10's ability to form tribo films between contacting surfaces, effectively reducing metal-to-metal contact, friction, and wear.
- Dynamic performance of MR shock absorbers filled with the bio-based fluids was analysed using:
    - Counterfeit simulations via multi-physics finite element analysis (FEA).
    - Experimental validation using a Universal Testing Machine (UTM) at 1.4 A current.
- SSO + 2.5 wt.% TL results:
    - Counterfeit analysis: 1690 N resisting energy, 9.28 resisting force ratio.
    - UTM exploratory test: 1780 N resisting energy, 10.47 resisting force ratio.
- CNSO + 2 wt.% TL results:
    - Counterfeit analysis: 1610 N, 9.04 ratio.
    - UTM exploratory test: 1710 N, 10.05 ratio.
- The error between simulation and experimental results was within acceptable limits:
    - SSO: ~9% energy error, ~10.2% force ratio error.
    - CNSO: ~10% error in both energy and force ratio.
- Molecular-level behavior of the oils was further interpreted using Spartan '18 software, leveraging electrostatic potential analysis to understand tribological enhancement mechanisms.
- Overall, the study confirms that bio-based MR fluids enhanced with Tergitol-NP10 are viable for mechanical applications such as shock absorbers, offering improved wear resistance and operational efficiency, and hold promise for further development.

## References

1. S. Mantripragada, X. Wang, F. Gordaninejad, B. Hu, and A. Fuchs, "Rheological properties of novel magnetorheological fluids," Int. J. Mod. Phys. B, vol. 21, pp. 4849–4857, 2007. [Online]. Available: https://doi.org/10.1142/s021797920704575x
2. J. Rabinow, "The Magnetic Fluid Clutch," Trans. Am. Inst. Electr. Eng., vol. 67, pp. 1308–1315, 1948. [Online]. Available: https://doi.org/10.1109/T-AIEE.1948.5059821
3. A. G. Olabi and A. Grunwald, "Design and application of magneto-rheological fluid," Mater. Des., vol. 28, pp. 2658–2664, 2007. [Online]. Available: https://doi.org/10.1016/j.matdes.2006.10.009
4. T. Biswal and L. B. Rao, "Analysis of the magnetic field for MR damper working in shear mode," Int. J. Struct. Eng., vol. 7, pp. 48–62, 2016. [Online]. Available: https://doi.org/10.1504/IJSTRUCTE.2016.073678
5. J. Wang and G. Meng, "Magnetorheological fluid devices: Principles, characteristics and applications in mechanical engineering," Proc. Inst. Mech. Eng. Part L: J. Mater. Des. Appl., vol. 215, pp. 165–174, 2001. [Online]. Available: https://doi.org/10.1243/1464420011545012
6. S. B. Lu, Y. N. Li, S. B. Choi, L. Zheng, and M. S. Seong, "Integrated control on MR vehicle suspension system associated with braking and steering control," Veh. Syst. Dyn., vol. 49, pp. 361–380, 2011. [Online]. Available: https://doi.org/10.1080/00423110903401889

7. J. Seok, S. O. Lee, K. I. Jang, B. K. Min, and S. J. Lee, "Tribological properties of a magnetorheological (MR) fluid in a finishing process," Tribol. Trans., vol. 52, pp. 460–469, 2009. [Online]. Available: https://doi.org/10.1080/10402000802687932
8. B. G. Shetty and P. S. S. Prasad, "Rheological Properties of a Honge Oil-based Magnetorheological Fluid used as Carrier Liquid," Def. Sci. J., vol. 61, pp. 583–589, 2011. [Online]. Available: https://doi.org/10.14429/dsj.61.331
9. J. Huang, J. Q. Zhang, Y. Yang, and Y. Q. Wei, "Analysis and design of a cylindrical magneto-rheological fluid brake," J. Mater. Process. Technol., vol. 136, 2018. [Online]. Available: https://doi.org/10.1016/S0924-0136(02)00634-9
10. N. J. Fox and G. W. Stachowiak, "Vegetable oil-based lubricants—A review of oxidation," Tribol. Int., vol. 40, pp. 1035–1046, 2007. [Online]. Available: https://doi.org/10.1016/j.triboint.2006.10.001
11. N. Golinelli and A. Spaggiari, "Experimental validation of a novel magnetorheological damper with an internal pressure control," J. Intell. Mater. Syst. Struct., vol. 28, pp. 2489–2499, 2017. [Online]. Available: https://doi.org/10.1177/1045389X17689932
12. G. Hu, H. Liu, J. Duan, and L. Yu, "Damping performance analysis of magnetorheological damper with serial-type flow channels," Adv. Mech. Eng., vol. 11, pp. 1–12, 2019. [Online]. Available: https://doi.org/10.1177/1687814018816842
13. T. M. Gurubasavaraju, H. Kumar, and A. Mahalingam, "An approach for characterizing twin-tube shear-mode magnetorheological damper through coupled FE and CFD analysis," J. Braz. Soc. Mech. Sci. Eng., vol. 40, 2018. [Online]. Available: https://doi.org/10.1007/s40430-018-1066-z
14. S. Li, W. Meng, and Y. Wang, "Numerical and experimental studies on a novel magneto-rheological fluid brake based on fluid–solid coupling," Sci. Prog., vol. 103, 2020. [Online]. Available: https://doi.org/10.1177/0036850419879000
15. N. H. Jayadas and K. P. Nair, "Coconut oil as base oil for industrial lubricants—Evaluation and modification of thermal, oxidative and low temperature properties," Tribol. Int., vol. 39, pp. 873–878, 2006. [Online]. Available: https://doi.org/10.1016/j.triboint.2005.06.006